Chemistry–A European Journal
Research Article
doi.org/10.1002/chem.202403422
Chemistry Europe
European Chemical Societies Publishing
www.chemeurj.org

Flipping the Metalation of 4-Dimethylaminopyridine: Steric Repulsion versus London Dispersion Attraction

Valery A. Verkhov,[b] Alexandra N. Gubanova,[b] Daria I. Tonkoglazova,[b] Elena Yu. Tupikina,[b] and Alexander S. Antonov*[a]

Non-covalent interactions, including the coordination of an organolithium reagent by a directing group and the steric hindrance from substituents, play a crucial role in determining the selectivity of metalation reactions. Here, we demonstrate the effective utilization of steric interactions for flipping the lithiation of 4-dimethylaminopyridine (DMAP). Introduction of a Me_3Si substituent to the position 1 of DMAP or simple complexation with *t*-BuLi allows selective C3-lithiation, due to the steric hindrance of a C2–H bond by the bulky moiety at the pyridine nitrogen. This simple approach creates a convenient way to achieve the selective C3-functionalization of DMAP. In contrast, the utilization of an even bulkier *i*-Pr_3Si substituent leads to exclusive C2-functionalization due to the dispersion interactions with organometallic bases. For the first time, it is demonstrated that the *i*-Pr_3Si moiety can serve as a directing group, providing a new type of directed *ortho*-metalation effect.

Introduction

Pyridines are among the most common heterocyclic structural units in pharmaceuticals and agrochemicals. They are a scaffold for over 7000 known natural compounds and commercial drugs.[1,2] Outstanding diversity of biological activity provided by the pyridine core naturally leads to the constant development of novel methods for its construction and functionalization. The advent of organometallic chemistry and especially of transition metal catalysis dramatically boosted this research field and provided the possibility to construct virtually any pyridine-based compound.[3–5] However, despite the grand success of homogeneous catalysis, the high cost of metals like palladium, platinum, and rhodium, along with the need for complex and expensive ligands, as well as challenges in purifying the final products from toxic transition metals, continue to limit its application. This is especially crucial for large-scale pharmaceutical production, where cost-effectiveness and high purity (specifically the content of transition metal traces) are of great importance. At the same time, the main group organometallics, particularly organolithiums, lack these disadvantages. Consequently, they not only maintain their solid positions as indispensable tools for modern organic synthesis but also open up new possibilities through novel applications discovered in recent years.[6,7] Although lithium must be removed from industrial wastewater after product separation, this disadvantage is more than compensated by the above-mentioned advantages of organolithium reagents. It comes as no surprise that nowadays, it is almost impossible to imagine an industrial multistep synthesis of biologically active and natural compounds without the utilization of organolithiums during at least one step.[8,9]

Naturally, functionalization of commercially available pyridines via reactions with organolithiums appears to be an excellent alternative to the classical methods (based on condensation reactions, and is heavily restricted by the structure of the initial reagents) and transition metal catalyzed transformations.[10] Due to the high CH-acidity of pyridines (in comparison with benzenes), they are perfect substrates for the functionalization via initial lithiation. However, this valuable feature of pyridines is significantly limited by their tendency to undergo nucleophilic addition of polar organometallic reagents.[11] This problem was to some extent solved by using weakly nucleophilic organometallic reagents, such as LDA and lithium tetramethylpipyridine (LTMP), while simultaneously increasing the CH-acidity through quaternization of the pyridine nitrogen atom (Scheme 1a).[12]

An even more elegant approach is the utilization of a mixture of *n*-BuLi with lithium dimethylaminoethanol (LiDMAE)–the so-called Caubère's salt (Scheme 1b).[13] All of these methods enabled the selective metalation of pyridines at position 2(6), leaving the functionalization of other positions inaccessible via lithiation. The exceptions are the formation of 4-lithiopyridines via the metalation of pyridine with Schlösser superbase in the presence of HMPA and the lithiation of 2,6-bis(triethylsilyl)pyridine with *n*-BuLi in the presence of PMDTA (Scheme 1c).[14,15]

Activation of the other positions of the pyridine ring has become feasible using the directed *ortho*-metalation (DOM) effect, provided by substituents (Scheme 1d). The DOM-effect is

[a] A. S. Antonov
Institute of Organic Chemistry, University of Regensburg, D-93053 Regensburg, Germany
E-mail: Alexander.Antonov@chemie.uni-regensburg.de
[b] V. A. Verkhov, A. N. Gubanova, D. I. Tonkoglazova, E. Y. Tupikina
Institute of Chemistry, St. Petersburg State University, 198504St. Petersburg, Russian Federation

Supporting information for this article is available on the WWW under https://doi.org/10.1002/chem.202403422

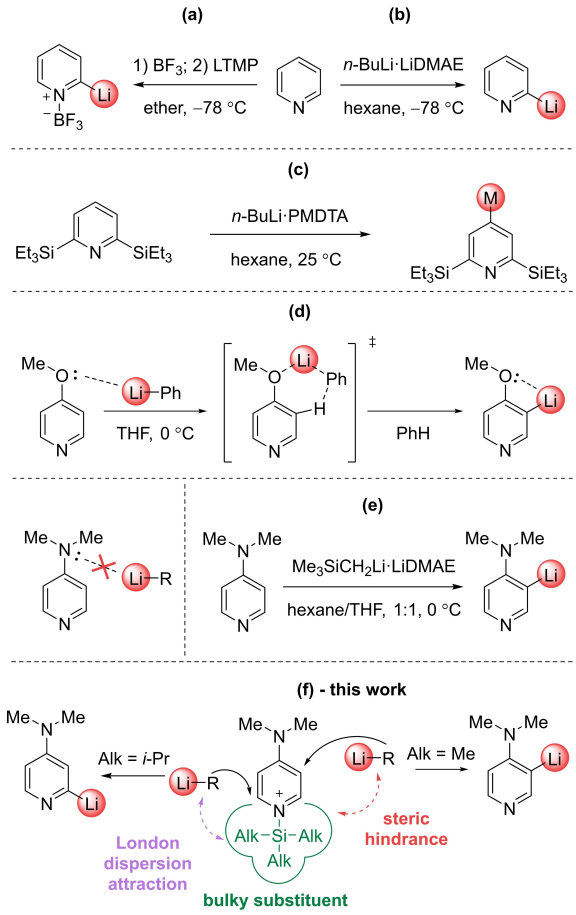

Scheme 1. Regioselective metalation of pyridines: C2–H lithiation with LTMP (a) and *n*-BuLi·LiDMAE (b) driven by high CH-acidity; exceptional case of C4–H lithiation via steric hindrace of C3–H bond by bulky substituents in positions 2 and 6 (c); C3–H lithiation of 4-methoxypyridine via DOM-effect (d); C3–H lithiation of 4-dimethylaminopyridine, which is unable to provide a DOM-effect, with Me_3SiCH_2Li·LiDMAE driven by enhanced CH-acidity (e); our approach of selective C3–H and C2–H lithiation based on repulsive and attractive interactions of organometallic reagent with bulky substituent (f).

manifested via the coordination of the organometallic reagent to the lone electron pair of the directing group, which facilitates the deprotonation of the CH–bond in the *ortho*-position relative to this group.[16] In contrast to carbocycles, the presence of a nitrogen atom in a pyridine core leads to the conjugation-driven transition of the electron density from the substituent into the ring. As a result, only groups containing more than one lone electron pair are able to effectively coordinate the organometallic reagent and provide the DOM-effect.[17,18] Thus, while 4-methoxypyridine is easily metalated to position 3, 4-dimethylaminopyridine (DMAP) undergoes selective metalation with common organolithium reagents in position 2.[19,20] To the best of our knowledge, the only known way to achieve the metalation of DMAP in position 3 is to utilize sterically hindered Caubère's salt – a mixture of trimethylsilylmethyllithium with LiDMAE (Scheme 1e).[21] At the same time, the most straightforward approach based on the steric inhibition of C2–H bond metalation and thus favoring C3–H functionalization remains unexplored.

It was previously shown that the introduction of bulky substituents, such as trimethylsilyl groups, into dimethylaniline and even anisole molecules allows one to change the direction of metalation reactions relying on the so-called "buttressing effect". Thus due to steric blocking of the most acidic C2–H bond, mainly the C3–H bond was subjected to metalation.[22,23] Keeping this in mind, the steric suppression of DMAP metalation at position 2(6) via the introduction of a bulky substituent to the pyridine nitrogen atom appears to be an elegant way to enable the functionalization of position 3(5) with organometallic reagents (Scheme 1f). This approach is very beneficial since the quaternization of pyridines with trialkylsilyl groups can simply be achieved in an *in situ* manner.[24,25] At the same time, this approach additionally increases the CH-acidity, thus allowing the utilization of weakly nucleophilic organometallic reagents, such as LDA and LTMP. In total, this would allow a simple, effective, and tunable functionalization of pyridines to position 3(5) under mild conditions without the necessity of permanent introduction of directing groups.

Results and Discussion

The ease of the lithiation of any organic compound depends on the CH-acidity of the corresponding bond. The presence of a heteroatom in a pyridine ring significantly polarizes neighboring C2(6)H–bonds, facilitating their lithiation. At the same time, the introduction of electron donating groups strongly conjugated with the heterocycle, such as OMe and NMe_2, dramatically changes charge distribution and thus acidities of CH–bonds. The latter is additionally affected if pyridine nitrogen is subjected to quaternization (i.e. alkylation, acylation, silylation, etc.). With this in mind, our study began with evaluating the distribution of electron density in 4-dimethylaminopyridine (DMAP) and *N*-trimethylsilyl-4-dimethylaminopyridine (Me_3Si-DMAP) and their ability to interact with organolithium reagents.

The planarization of the nitrogen atom of the dimethylamino group is an effective descriptor of the degree of conjugation with the pyridine ring. It can be effectively estimated as the deviation of the sum of the angles at the nitrogen atom from 360° ($\Delta\varphi$, Table 1). The closer this indicator is to zero, the higher the degree of sp^2-hybridization of the nitrogen atom of the dimethylamino group, and therefore the higher the degree of its conjugation with the heteroring. Alternatively, this can be determined through the residual electron density on the nitrogen atom of the NMe_2 group. This can be visualized using the electron localization function (ELF) (shown in yellow, Figure 1a).[26] The more the lone electron pair is conjugated, the lower is the maximum ELF value: ELF = 1 corresponds to a perfect lone pair localization, while ELF = 0.5 corresponds to a fully delocalized lone pair (so-called electron gas). In addition to DMAP and Me_3Si-DMAP, an *N,N*-dimethylaniline (DMA) molecule was analyzed in a similar way for comparison.

It should be noted that in contrast to DMA, both $\Delta\varphi$ and max ELF values of DMAP strongly depend on the dielectric constant of the used solvent. Thus, when moving to more polar solvents these values decrease, which indicates conjugation

Table 1. Conjugation parameters of the dimethylamino group and the aromatic ring of the compounds under study at various dielectric constant values (ε). b3lyp/6-311 + + g(d,p) empiricaldispersion = gd3 scrf = (cpcm, solvent).

Solvent	ε	Δφ, °[a]			Max ELF[b]			Econj, kJ/mol[c]	
		DMA	DMAP	Me_3Si-DMAP	DMA	DMAP	Me_3Si-DMAP	DMA	DMAP
Vacuum[d]	1.0	5.1	2.0	0.0	0.92	0.90	0.86	177	209
Hexane	1.9	5.3	1.4	0.0	0.92	0.90	0.86	180	219
Benzene	2.3	5.3	1.3	0.0	0.92	0.90	0.86	181	222
Et_2O	4.2	5.3	0.9	0.0	0.92	0.89	0.86	183	229
THF	7.4	5.3	0.6	0.0	0.92	0.89	0.86	185	234
–[e]	100	5.2	0.2	0.0	0.92	0.88	0.86	186	240

[a] The difference between 360° and the sum of the angles at the nitrogen atom of the dimethylamino group. [b] The maximum value of the electron localization function corresponding to the residual electron density on the nitrogen atom of the dimethylamino group. [c] Highest stabilization energy E(2) between the lone electron pair of the nitrogen atom of the dimethylamino group (LP) and the 2-center antibonding non-Lewis orbital (BD*) obtained using second order perturbation theory in the framework of NBO approach. [d] Without using the SCRF method. [e] The solvent is not included in the Gaussian solvent set. Only the value of its dielectric constant (ε) is indicated.

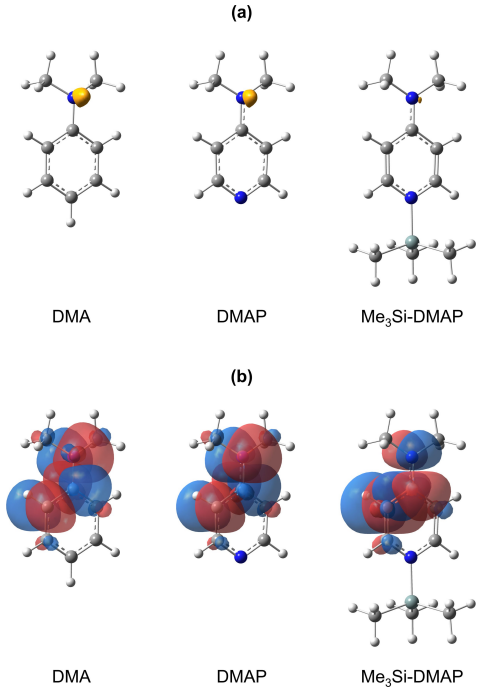

Figure 1. Optimized geometries of DMA, DMAP and Me_3Si-DMAP with visualization of the electron localization function (ELF) (shown in yellow) of the nitrogen atom of the dimethylamino group, ELF = 0.85 (a) and visualization of the analysis of natural bond orbitals, isovalue = 0.02 (b). Quaternization of pyridine nitrogen leads to the decrease of the ELF value on the nitrogen atom of the NMe_2 group due to the strong conjugation, thus preventing the realization of the DOM-effect. B3LYP–D3/6-311 + + G(d,p) (CPCM=THF).

strengthening of the dimethylamine group with the heteroring. This is explained by the stabilization of separated charges in the more polar solvents.

While the dimethylamino group of DMA is significantly planarized, its lone electron pair is still noticeably localized (Δφ = 5°, max ELF = 0.92). This is sufficient for the effective coordination of an organometallic reagent to provide directed *ortho*-metalation. Even though absolute values of Δφ and max ELF do not drastically change upon transition to DMAP, the latter is unable to exhibit the DOM-effect. Since even in DMA the NMe_2 group is already significantly planarized, a further 3° reduction of the Δφ value and a 0.02 units reduction of the max ELF value in vacuum dramatically affects the availability of this group for the coordination of an external organometallic reagent.

Transition to Me_3Si-DMAP additionally contributes to the above-mentioned tendency. As a result, the dimethylamino group is completely conjugated with the pyridine ring and is planar (Δφ = 0°). At the same time, the max ELF value drops to 0.86. Changing the dielectric constant of the solvent, in this case, has no effect, thus the conjugation achieves the maximum possible degree here.

Additionally, we investigated the impact of the introduction of F_3B and *i*-Pr_3Si groups to the pyridine nitrogen of DMAP. It was found that regardless of the introduced group, the Δφ parameter is close to zero (see Table S1 in SI), and the max ELF value varies in a narrow range: 0.87–0.85 (see Table S2 in SI). For a more complete description, we additionally analyzed the total rotational energy of the dimethylamino group relative to the plane of the ring (see Table S3 in SI), the bond length between the nitrogen atom of the dimethylamino group and the ring carbon atom (see Table S4 in SI) and the natural valence level occupancy of the nitrogen atom of the dimethylamino group (see Table S5 in SI). These parameters maintained the general trend, although they changed as monotonously as the max ELF parameter, thus not allowing to drawing clear borders between systems capable and incapable of providing the DOM-effect. More informative in this regard is the analysis of natural bond orbitals (NBO) (Figure 1b). To estimate the degree of conjugation of the NMe_2 group with the aromatic ring, we used the highest conjugation energy (E_{conj}, kJ/mol) of the lone electron pair of the nitrogen atom of the NMe_2 group (LP) with the 2-center antibonding non-Lewis orbital (BD*), which belongs to the C–C bond of the ring and is 99.96% p-character. For DMA the E_{conj} value changes in the range of 177–186 kJ/mol, while transitioning to DMAP shifts the range to 209–240 kJ/mol (Table 1). Thus, the E_{conj} value serves as the best descriptor of the possibility of DOM-effect manifestation.

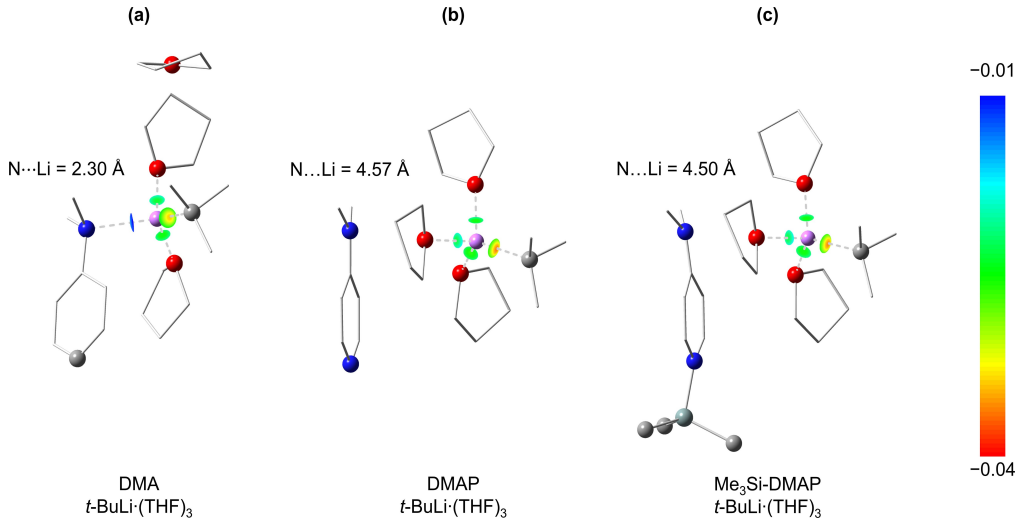

Figure 2. Optimised geometries of complexes obtained after the interaction of DMA (a), DMAP (b) and Me_3Si-DMAP (c) with *t*-BuLi·$(THF)_3$. The OTf anion and hydrogen atoms are omitted for clarity. Isosurfaces of interaction region indicator (IRI = 1.1) around lithium atoms mapped by $sign(\lambda_2)\rho$ demonstrate weak attraction between lithium and nitrogen of DMA and strong attraction of *t*-Bu carbon and THF oxygen. Selected interatomic distances are given: upon interaction with *t*-BuLi·$(THF)_3$, the DMA molecule substitutes THF in the coordination sphere of lithium; DMAP and Me_3Si-DMAP stay out of the coordination sphere of lithium. B3LYP–D3/6-311 + + G(d,p) (CPCM=THF).

However, when moving to DMAP with a substituent in the position 1 (F_3B-DMAP, Me_3Si-DMAP, *i*-Pr_3Si-DMAP), the electron pair becomes so delocalized that it leads to the absence of the LP orbital of the nitrogen atom of the dimethylamino group in the NBO analysis (shown on the example of Me_3Si-DMAP, Figure 1b). Naturally, comparing the conjugation energies of orbitals for these systems does not make physical sense.

Finally, the interaction of the dimethylamino group of DMA, DMAP, and Me_3Si-DMAP with the complex *t*-BuLi·$(THF)_3$ was simulated. The starting geometry for all systems was similar: the lithium atom was surrounded by 5 ligands positioned at equal distances (2 Å). Optimized geometries of the resulting systems are given in Figure 2. Since interatomic distance is not a solid criterion of the interaction, the latter was assessed by the value $sign(\lambda_2)\rho$ on the interaction region indicator (IRI) isosurface (Figure 2).[27,28] As a result, only in the case of DMA, a weak attraction (van der Waals interaction) of the dimethylamino group and the organolithium reagent occurs (based on the values of $sign(\lambda_2)\rho$ on the IRI isosurface). On the contrary, the NMe_2 groups of DMAP and Me_3Si-DMAP molecules refrain from entering the coordination sphere of lithium.

Altogether, the quaternization of the pyridine nitrogen atom in general leads to the strengthening of the conjugation of the dimethylamino group with the heteroring and disables its ability to coordinate the organometallic reagent, which leaves no room for the manifestation of the DOM-effect. Thus, chemical interactions of DMAP and its 1-substituted derivatives (F_3B-DMAP, Me_3Si-DMAP, *i*-Pr_3Si-DMAP, etc.) with organolithium reagents are controlled only by acidity and steric accessibility of the corresponding CH–bond.

To evaluate the steric accessibility of the protons of the pyridine ring for metalation reactions, we have developed a new method. This method consists of calculating the area belonging to a particular atom (atomic basins) on the isosurface of electron density (0.001 a.u.).[29] The boundaries of the basin of pyridine protons of the aromatic ring are set by the conditions of zero flux of the electron density gradient (Figure 3). The relative availability of protons in positions 2(6) and 3(5) of the pyridine ring can be illustrated by the S_{2H}/S_{3H} ratio (Scheme 2). Thus, in a DMAP molecule, the average accessible surface area of the proton at position 2 (S_{2H} = 11.8 Å^2) is 1.4 times larger than the average accessible surface area of the proton at position 3 (S_{3H} = 8.5 Å^2). The addition of substituents to the pyridine nitrogen reduces the steric availability of protons at positions 2 and 6. Regardless of the substituent in position 1, the surface area of the protons in position 3 remains almost unchanged (see Table S6 in SI).

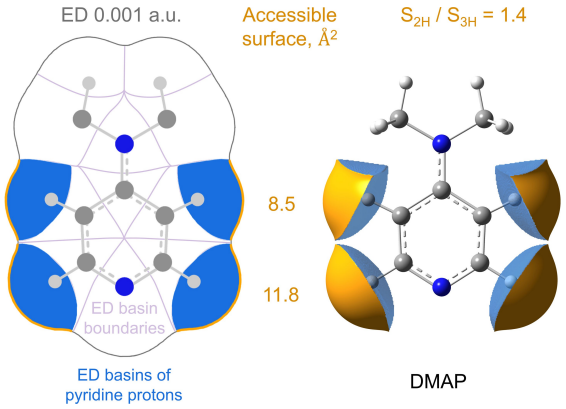

Figure 3. The accessible surface area of pyridine protons in DMAP, acquired by the intersection of the electron density (ED) isosurface of 0.001 a.u. and the electron density (ED) basins of the corresponding atoms. The relative ratio of accessible surface areas of C2–H and C3–H protons (S_{2H}/S_{3H}) shows a much higher steric availability of C2(6)–H bonds. The accessibility of C3(5)–H bonds is sterically hindered by the planarized NMe_2 group. B3LYP–D3/6-311 + + G(d,p) (CPCM=THF).

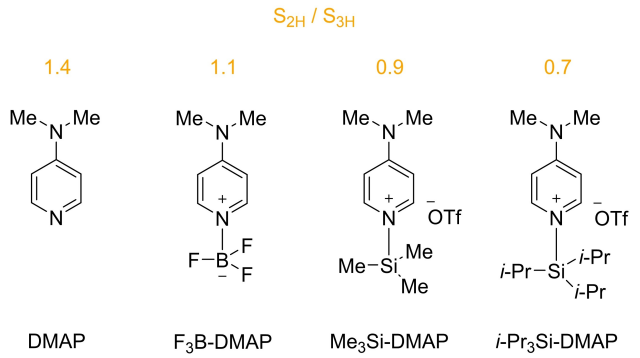

Scheme 2. The S_{2H}/S_{3H} ratio of pyridine hydrogen atoms, Å^2. Introduction of a substituent to the position 1 reduces the steric availability of C2(6)–H bonds, consequentially making C3(5)–H bonds more available for the interaction. B3LYP–D3/6-311++G(d,p) (CPCM=THF).

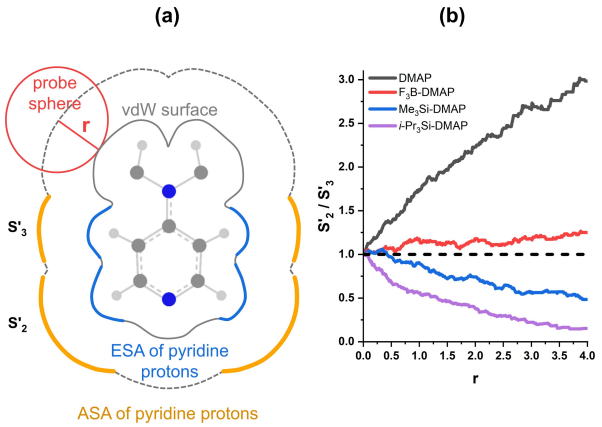

Figure 4. The accessible surface area (ASA) of pyridine protons formed by the center of the probe sphere rolling on the van der Waals (vdW) surface specified by the vdW radii of the atoms, at the points of contact with the excluded surface area (ESA) of the pyridine protons. Utilization of larger reagents provides better differentiation of steric availability of pyridine protons facilitating the interaction with C3(5)–H bonds in the case of 1-substituted DMAPs. B3LYP–D3/6-311++G(d,p) (CPCM=THF).

Surprisingly, while the Me_3Si substituent is much larger than BF_3 due to the longer Si–N bond (1.87 Å) in comparison with the B–N bond (1.64 Å), both F_3B-DMAP and Me_3Si-DMAP molecules are characterized by their similar S_{2H}/S_{3H} values of 1.1 and 0.9, respectively. Based on this, utilization of the Me_3Si group can be potentionally not sufficient to provide a significant difference in the availability of pyridine protons for the organometallic reagent. In contrast, the bulkier *i*-Pr_3Si group provides much better means of distinguishing the steric accessibility of pyridine protons ($S_{2H}/S_{3H}=0.7$).

The outcome of the actual metalation reaction depends on both the steric availability of the electron density of the proton and the size of the organometallic reagent. To take the latter into account the method of rolling a probe sphere was used.[30,31] In this approach, the sphere serves as a geometrically simplified organometallic reagent. This sphere is rolled over the surface, determined by the van der Waals radii of the atoms. As a result, the center of a given sphere describes the accessible surface of the molecule for a sphere with a given radius (Figure 4a).

The absolute values of the accessible surface S′ obtained by this method are given in Figure S2 in SI. However, it is more informative to compare the ratio S'_{2H}/S'_{3H}. In this method, when the radius of the probe sphere is equal to 0, the accessibility of all atoms is close and their ratio S'_{2H}/S'_{3H} is equal to 1 (Figure 4b). This is due to the fact that the ball rolls over the van der Waals surface, determined from the van der Waals radii, which are the same for the same atoms. However, as soon as the probe sphere acquires a noticeable size, the accessibility of positions changes. Thus, protons at positions 2(6) in DMAP and F_3B-DMAP molecules are more accessible for the organometallic reagent. When moving to Me_3Si-DMAP and *i*-Pr_3Si-DMAP, position 3 becomes more sterically accessible. In general, the larger the substituent at position 1 becomes, the more preferable position 3 becomes. Utilization of bulkier organometallic reagents provides an even better S'_{2H}/S'_{3H} ratio.

Finally, in addition to the steric accessibility, the strength (see Table S7 in SI) and polarity of CH bonds play a key role in metalation reactions. CH-polarity can be estimated by the distance (Δd, Å) between the minima of electron density (ED_{min}) and electrostatic potential (ESP_{min}), along the bond path (d(BP), Å) (see Table S8 in SI).[32] For the CH bonds of studied compounds, ESP_{min} is located closer to the carbon atom than ED_{min} (Figure 5). This indicates that the carbon atom has a more negative charge than the hydrogen atom, which is in better agreement with the actual electronic structure of studied molecules than the results of calculation of CH-acidities based on atomic charges (see Table S9–10 in SI). The greater the distance between the minima Δd, the more polar the CH bond will be, and therefore, it will be easier for it to undergo metalation reactions. However, the length of the bond path d(BP) does not remain constant, so it is more appropriate to use not the absolute, but the relative value: $\delta=(\Delta d\cdot 100\,\%)/d(BP)$ (Table 2).

Overall, performed calculations demonstrate that DMAP and its 1-substituted derivatives are incapable of providing a DOM-effect, thus their metalation is controlled by the acidity and steric availability of CH–bonds. Quaternization of the pyridine nitrogen atom increases the polarity of all CH bonds, especially the C2–H bond. The usage of bulky substituents, such as Alk_3Si,

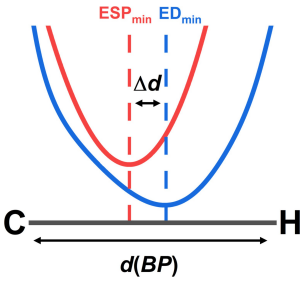

Figure 5. Schematic representation of a CH bond path. CH-polarity can be estimated by the distance (Δd, Å) between the minima of electron density (ED_{min}) and electrostatic potential (ESP_{min}), along the bond path (d(BP), Å). Greater distance between the minima Δd corresponds to higher polarity of the C–H bond.

Table 2. Relative distance (δ = (Δd·100%)/d(BP)) between the ED and ESP minima along the C–H bond path of DMAP and its derivatives. Introduction of a substituent in position 1 increases polarity of all C–H bonds, keeping C2–H bond the most polar in all cases.

Molecule	δC2–H, %	δC3–H, %
DMAP	0.64	0.46
F_3B-DMAP	1.84	0.95
Me_3Si-DMAP	1.63	1.12
i-Pr_3Si-DMAP	1.58	1.11

hinders the accessibility of C2–H protons favoring the deprotonation of the C3–H bond.

To experimentally test our theoretical findings, we investigated the interaction of DMAP and its 1-substituted derivatives with non-nucleophilic strong organometallic bases: lithium diisopropylamide (LDA) and lithium tetramethylpiperidide (LTMP). The formation of lithiated species was detected by quenching the reaction mixture with DMF, leading to the formation of corresponding aldehydes, which are easily detectable in ^{1}H NMR spectra (Figure 6).

Due to the low polarity of CH–bonds, DMAP does not react with LDA or LTMP even at room temperature (Table 3, runs 1–4) as expected. In contrast, BF_3–DMAP prepared *in situ* undergoes selective metalation at position 2 (runs 5–9). In some cases, when the excess of the organometallic base is utilized, the 2,6-dimetalation occurs, giving corresponding aldehydes **1 a** (R=CHO) and **2 a** (R=CHO) (runs 7,8), which is in agreement with previous studies.[12]

As it was predicted by our calculations, Me_3Si-DMAP prepared *in situ* undergoes selective metalation at position 3: no traces of 2-substituted products are observed (runs 10–14). Noticeably, no aldehydes can be detected in the ^{1}H NMR spectra of crude reaction mixtures since the reaction of initially formed lithiated species with DMF is intercepted by the transfer of the Me_3Si group from position 1 or from equilibrating the amount of free Me_3SiOTf. Thus, in these experiments, initially formed 3-lithioDMAP was detected in the form of Me_3Si derivative **3 b** (R=Me_3Si). It was not possible to reach an NMR yield of over 11% independently of the reaction conditions, due to the insufficient basicity of utilized reagents. Increasing the amount of the organometallic base does not provide any improvement; probably due to the higher aggregation of the reagents at higher concentrations.[33]

To our surprise, the reaction of *i*-Pr_3Si-DMAP containing a much bulkier substituent in position 1 (in comparison with Me_3Si-DMAP) with LDA or LTMP results in the selective metalation of the C2–H bond, providing product **1 b** (R = *i*-Pr_3Si) with a good NMR yield (runs 15–19). This unexpected C2–H selectivity and high conversion can only be attributed to intramolecular metalation via some kind of directing effect provided by the *i*-Pr_3Si group. The latter possesses no lone electron pairs, thus it is uncapable to direct the organolithium reagent via coordination of lithium (classical DOM-effect). At the same time, the *i*-Pr_3Si moiety is well known for its strong dispersion interactions that dramatically affect reaction performance.[34–39] We believe that the *i*-Pr_3Si group of *i*-Pr_3Si-DMAP can be involved in London dispersion interactions with LDA and LTMP, which are rich with CH bonds – a key requirement for an effective dispersion interaction (Scheme 3). This interaction leads to the formation of a reactive complex with the proximity of the C2–H bond and the organometallic base. Further deprotonation occurs in a semi-intramolecular manner (inside the dispersion-bonded complex), which explains high yields.

To examine the ability of trialkylsilyl groups of Alk_3Si-DMAPs to participate in dispersion interactions, we again turned to theoretical modeling. For Me_3Si-DMAP and *i*-Pr_3Si-DMAP, the van der Waals potential (vdW potential) was constructed: the exchange-repulsion term is shown in grey and the dispersion term is shown in orange (Figure 7).[40] This represents the energy of the interaction with a helium atom as a test particle. The interaction energy of ±2.1 kJ/mol was chosen to separate the dispersion contribution of the aromatic ring from the methyl groups of the trialkylsilyl substituent (for details, Figure S3 and Table S11 in SI). Comparing the vdW potential for Me_3Si-DMAP and *i*-Pr_3Si-DMAP, one can observe that the regions of attractive dispersion interaction are located above and below the plane of the pyridine ring, as well as in the proximity of the methyl groups of the trialkylsilyl substituent. The main difference worth paying attention to is the difference in volumes of the dispersion region – for *i*-Pr_3Si-DMAP, this region near the methyl

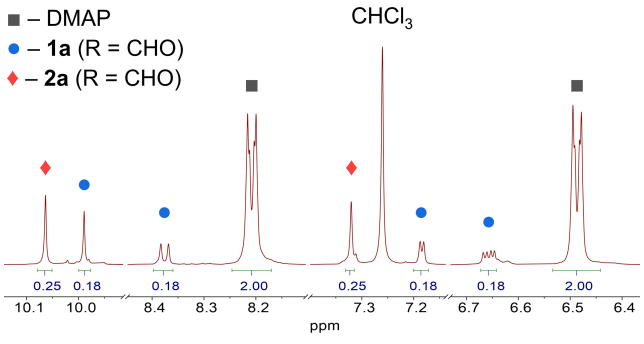

Figure 6. Aromatic region of a typical ^{1}H NMR spectrum (400 MHz, $CDCl_3$) of the reaction mixture obtained by the metalation of DMAP and its 1-substituted derivatives with organometallic bases followed by quenching with DMF (Table 4, run 7). Clear signal separation allows the determination of conversion and regioselectivity.

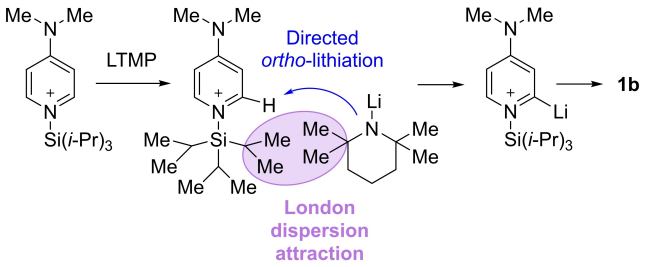

Scheme 3. Lithiation of *i*-Pr_3Si-DMAP with LTMP occurring via the formation of the London-dispersion-bonded complex: the *i*-Pr_3Si group provides a directing effect based on the dispersion interactions, facilitating selective *ortho*-metalation.

Table 3. Metalation of DMAP and 1-substituted DMAPs with LDA and LTMP.

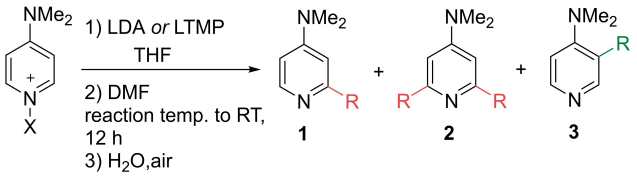

Run	X	Conditions	R	NMR yield, %		
				11	22	33
1	–	10 eq. LDA, −78 °C, 6 h	–	–	–	–
2	–	10 eq. LDA, +25 °C, 6 h	–	–	–	–
3	–	10 eq. LTMP, −78 °C, 1 h	–	–	–	–
4	–	10 eq. LTMP, +25 °C, 24 h	–	–	–	–
5	BF_3	10 eq. LDA, −78 °C, 1 h	CHO	38	–	–
6	BF_3	10 eq. LTMP, +25 °C, 20 h	CHO	–	–	–
7	BF_3	10 eq. LTMP, −78 °C, 1 h	CHO	14	10	–
8	BF_3	2 eq. LTMP, −78 °C, 1 h	CHO	7	2	–
9	BF_3	1.05 eq. LTMP, −78 °C, 1 h	CHO	51	–	–
10	Me_3Si	1.05 eq. LDA, −78 °C, 1 h	Me_3Si	–	–	10
11	Me_3Si	10 eq. LDA, −78 °C, 1 h	Me_3Si	–	–	6
12	Me_3Si	10 eq. LDA, −78 °C, 6 h	Me_3Si	–	–	6
13	Me_3Si	10 eq. LDA, +25 °C, 6 h	Me_3Si	–	–	11
14	Me_3Si	1.05 eq. LTMP, −78 °C, 1 h	Me_3Si	–	–	7
15	*i*-Pr_3Si	1.05 eq. LDA, −78 °C, 1 h	*i*-Pr_3Si	68	–	–
16	*i*-Pr_3Si	10 eq. LDA, −78 °C, 1 h	*i*-Pr_3Si	–	–	–
17	*i*-Pr_3Si	1.05 eq. LTMP, −78 °C, 4 h	*i*-Pr_3Si	39	–	–
18	*i*-Pr_3Si	10 eq. LTMP, −78 °C, 1 h	*i*-Pr_3Si	35	–	–
19	*i*-Pr_3Si	10 eq. LTMP, +25 °C, 24 h	*i*-Pr_3Si	77	–	–

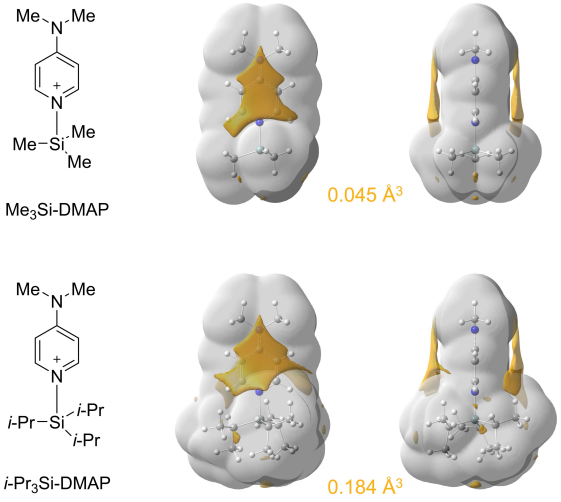

Figure 7. vdW potential isosurface of the interaction energy of Me_3Si-DMAP/*i*-Pr_3Si-DMAP and a He atom equal to ±2.1 kJ/mol. The gray region corresponds to the exchange-repulsion term, the orange ones to the dispersion term. The volume of the dispersion term region near the methyl groups of the trialkysyl substituent (orange number) suggest a much higher tendency of *i*-Pr_3Si-DMAP participating in dispersion interactions. B3LYP–D3/6-311++G(d,p) (CPCM=THF).

groups of the trialkysyl substituent is equal to 0.184 Å^3, which is 4.1 times larger than for Me_3Si-DMAP (0.045 Å^3). This indicates a higher probability of *i*-Pr_3Si-DMAP participating in dispersion interactions.

In the next step, we modeled the interaction of Alk_3Si-DMAPs with an organometallic reagent. The addition of a bare TMP anion results in a predominantly electrostatic interaction (Figure S4–5). That is why the organometallic reagent Li-$(THF)_3$TMP is modeled explicitly (Figure 8). For Me_3Si-DMAP, the transition from complex-1 with TMP in axial position (Figure 8a) to complex-2 with TMP in equatorial position (Figure 8b) is energetically unfavorable ($\Delta E = +5.4$ kJ/mol). In contrast, a similar transition for *i*-Pr_3Si-DMAP is favorable ($\Delta E = -0.3$ kJ/mol), which demonstrates the abovementioned stronger tendency of *i*-Pr_3Si-DMAP participating in dispersion interactions. We have compared the total electronic transition energies from complex-1 to complex-2 (ΔE, kJ/mol) for Me_3Si-DMAP and *i*-Pr_3Si-DMAP depending on the use of BJ damping function. The result shows that the absolute values of ΔE changes (see Table S12 in SI), the trend remains the same – attractive dispersion interactions are possible in case of *i*-Pr_3Si group ($\Delta E < 0$) and impossible for Me_3Si group ($\Delta E > 0$).

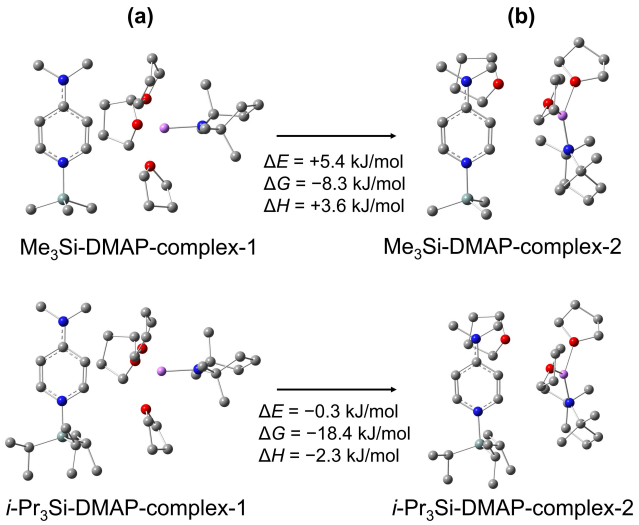

Figure 8. Optimized structures of $Li(THF)_3TMP$ complexes with Me_3Si-DMAP and *i*-Pr_3Si-DMAP. For *i*-Pr_3Si-DMAP, the transition from complex-1 to complex-2 is energetically favorable (ΔE = −1.5 kJ/mol), suggesting stronger dispersion interactions. B3LYP(BJ)-D3/6-311 + + G(d,p) (CPCM=THF).

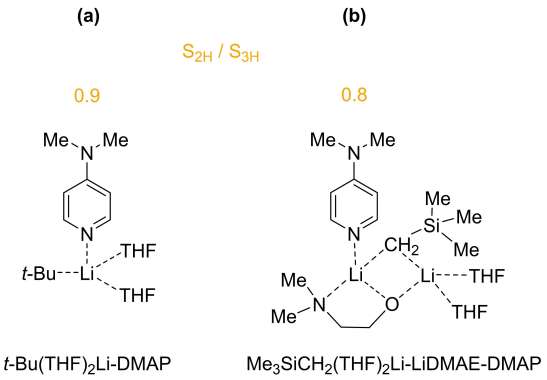

Scheme 4. The S_{2H}/S_{3H} ratio of pyridine hydrogen atoms, Å^2. The coordination of the organometallic reagent with pyridine nitrogen reduces the steric availability of C2(6)–H bonds and consequentially makes C3(5)–H bonds more available for the lithiation. B3LYP–D3/6-311 + + G(d,p) (CPCM=THF).

As it was mentioned above, the utilization of Me_3Si indeed allows to flip the metalation of DMAP and achieve selective C3-functionalisation. However, the low basicity of LDA and LTMP does not allow to reach reasonable yields. To address this issue, a more basic bulky *tert*-butyllithium was tested as a lithiating agent (Table 4). Due to the high nucleophilicity of organolithiums, pyridines are prone to undergo nucleophilic addition.[11] The quaternization of pyridine nitrogen additionally facilitates this addition. To address this issue, all experiments were performed at −78 °C. To our satisfaction, utilization of 10 equiv. of *t*-BuLi provides 3-substituted DMAP **3 a** with good NMR yield together with a smaller amount of the product of nucleophilic addition **4** (run 1). Usage of a smaller amount of *t*-BuLi gives less satisfactory results (runs 2–3). The transition to *i*-Pr_3Si-DMAP expectedly gives selective C2-functionalisation, due to the abovementioned directing effect of the *i*-Pr_3Si group (run 4).

We also tested the reaction of unsubstituted DMAP with *t*-BuLi. At −45 °C, the reaction proceeds exclusively as a nucleophilic addition (run 5), however to our surprise, at −78 °C, an excellent C3–H lithiation selectivity is achieved (run 6). It is important to note that, unlike the NMe_2 group of the DMAP molecule which lacks coordination abilities (see above), the aza–group can coordinate an organometallic reagent. Overall, the *t*-BuLi·THF_2 moiety coordinated to pyridine nitrogen acts similarly to the BF_3, $SiMe_3$ and *i*-Pr_3Si groups discussed above: it provides an increase in the conjugation of the dimethylamino group with the heteroring, polarization of CH–bonds, etc. (see Tables S1–S10 in SI). Most importantly, the *t*-BuLi·THF_2 moiety acts as a bulky substituent at position 1 that provides a steric hindrance to the interaction of the organometallic reagent with the C2(6)–H bond of the pyridine ring, (Scheme 4a) providing excellent selectivity of C3(5)–H bond lithiation.

To exclude the dispersion interaction with NMe_2 group as a directing force for C3–H lithiation, we performed additional calculations. To quantify the contribution of the NMe_2 group, the pyridine ring, and the trialkylsilyl group to the dispersion

Table 4. Metalation of DMAP and Me_3Si-DMAP with *t*-BuLi.

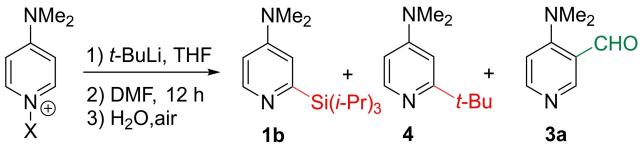

Run	X	Conditions	NMR yield,%		
			1 b	**4**	**3 a**
1	Me_3Si	10 eq. t-BuLi, −78 °C, 6 h	–	20	67
2	Me_3Si	3.0 eq. t-BuLi, −78 °C, 6 h	–	34	39
3	Me_3Si	1.0 eq. t-BuLi, −78 °C, 6 h	–	–	–
4	*i*-Pr_3Si	10 eq. t-BuLi, −78 °C, 6 h	91	–	–
5	–	10 eq. t-BuLi, −45 °C, 12 h	–	80	–
6	–	10 eq. t–BuLi, −78 °C, 12 h	–	–	91

interaction, we have divided electron density of the whole molecule along the boundaries of the electron density basins of the corresponding groups, which are limited by zero flux surfaces of atoms of this group (Figure S6 in SI). As a result, we obtained dispersion interaction isosurfaces at a certain energy associated with the electron density of the trialkylsilyl group, the pyridine ring, and the dimethylamino group separately. The volume contained within the isosurface of a dispersion interaction at a particular energy shows the regions of attraction where the absolute values of energy will be greater than or equal to the energy of the isosurface itself. Thus, the volumes of dispersion regions V for different groups at different values of E_{disp} can be calculated. Since the dependence $V(|E_{disp}|)$ is a rapidly decreasing function, we plotted the dependence $\sqrt[3]{V(|E_{disp}|)}$ for the sake of clarity (Figure S7 in SI). The region of the pyridine ring is sandwiched by the boundaries of the basins of the Alk_3Si and NMe_2 groups, so at low energies of attraction it gives the smallest contribution. However, as the E_{disp} increases, the volume of the dispersion region belonging to the pyridine ring starts to be larger than the volume of the NMe_2 group (for Me_3Si-DMAP at 0.6 kJ/mol, for *i*-Pr_3Si-DMAP at 0.7 kJ/mol), and then starts to exceed even the volume of the Alk_3Si group (for Me_3Si-DMAP at 0.9 kJ/mol, for *i*-Pr_3Si-DMAP at 1.5 kJ/mol). Nevertheless, compared to the NMe_2 group, the volume of the dispersive attraction regions of the Alk_3Si groups remains larger both for Me_3Si and *i*-Pr_3Si.

Although the pyridine ring gives a significant contribution to the dispersion interaction, it is necessary to note that, unlike nucleophilic addition reactions, metalation reactions will proceed through the side surface of the pyridine ring. Thus, it is more convenient to estimate the dispersion contribution from the side surface, but since this procedure is not precisely defined, then for a more accurate assessment, one can consider the van der Waals potential maps in the plane of the pyridine ring (Figure 9).

It is clear that the regions with larger $|E_{disp}|$ (green and blue regions in Figure below) are located mostly in concavity regions of van der Waals surface. Therefore, it is reasonable to expect that more sterically loaded groups are tend to participate in dispersion interaction. So, it is possible to measure the areas of the dispersion regions (S) with a change in energy (E_{disp}) for different groups. Since the dependence $S(|E_{disp}|)$ is also a rapidly decreasing function, then for clarity we will construct the dependences $\sqrt{S(|E_{disp}|)}$. With increasing energy, the area of the dispersion region belonging to the pyridine ring becomes larger only in comparison with the area of the NMe_2 group (for Me_3Si-DMAP at 0.7 kJ/mol, for *i*-Pr_3Si-DMAP at 0.8 kJ/mol). Trialkylsilyl groups have the largest dispersion areas, and the ratio of the area of these groups to the area of the NMe_2 group increases with increasing energy.

Thus, the dimethylamino group is a weaker dispersion interaction donor in comparison to trialkylsilyl groups. This is the possible reason why the metalation reactions of Me_3Si-DMAP are controlled by steric repulsion.

Finally, we have modelled the metalation reaction of DMAP in position 3 with *t*-BuLi·THF_3. The energy profile for this reaction is shown in Figure 10. It is clearly seen that for products, reactants, and transition state (TS), there is no indications of coordination of the *t*-Bu group to DMAP (interatomic distance between the carbon atom of the NMe_2 group and the carbon of the *t*-Bu group bonded to the lithium atom is 6.8 Å, 3.7 Å and 3.9 Å respectively, which exceed the

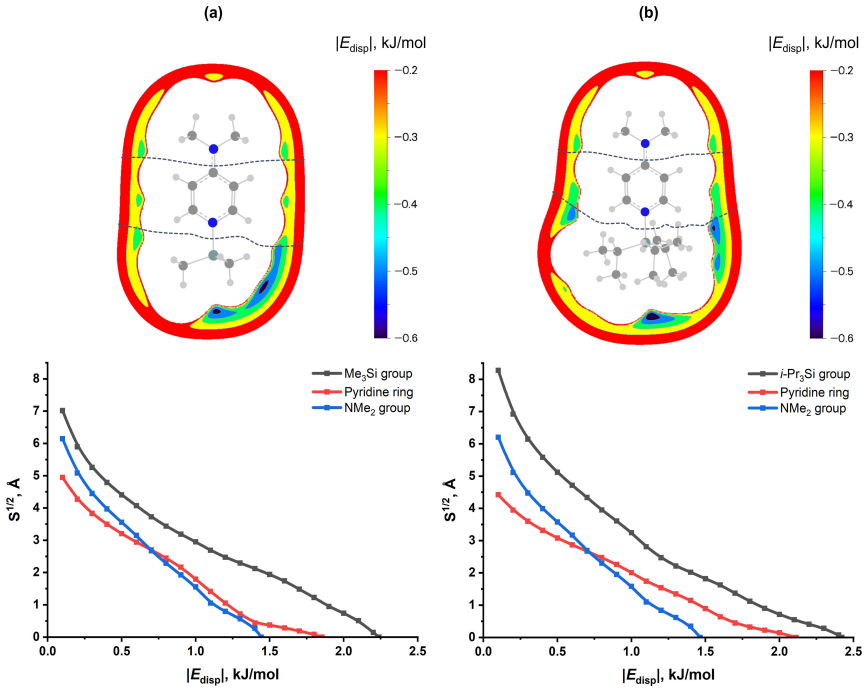

Figure 9. Dependence of the root of the area of dispersion regions in the plane of the ring for Me_3Si-DMAP (a) and *i*-Pr_3Si-DMAP (b) on the absolute value of the attractive energy: $\sqrt{S}-|Edisp|$. B3LYP–D3/6-311++G(d,p) (CPCM=THF).

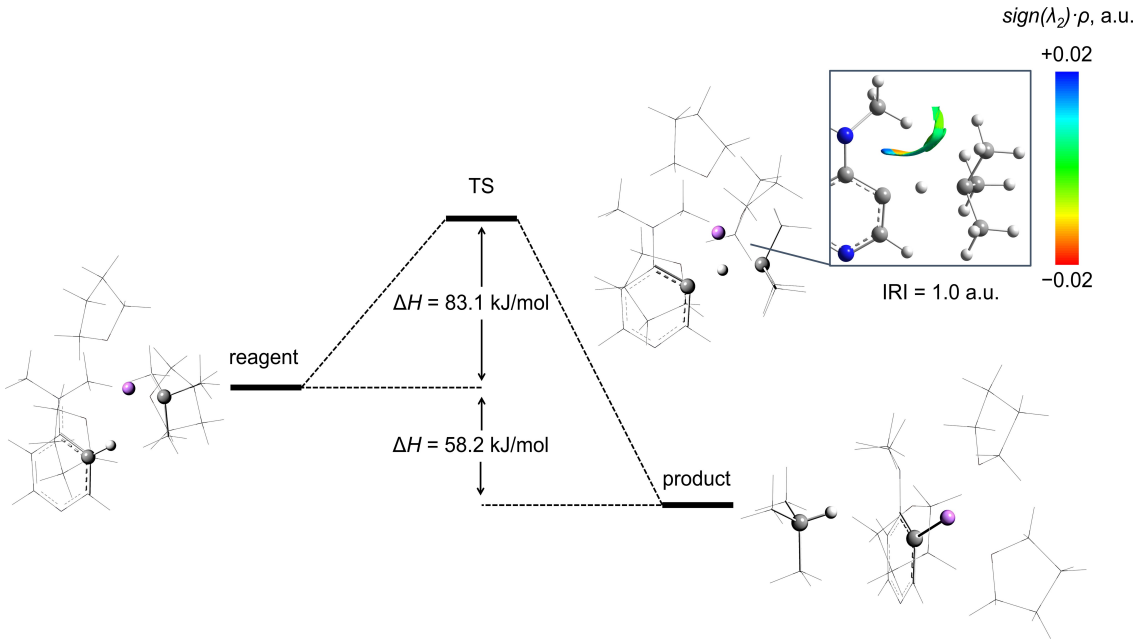

Figure 10. The energy profile of the metalation reaction of DMAP in position 3 with *t*-BuLi THF_3. B3LYP(BJ)-D3/6-311++G(d,p) (CPCM=THF).

sum of van der Waals radii $\Sigma_{vdw(C-C)} = 3.4$ Å, Bondi radii were used). For the transition state, we performed an additional study of the weak interactions by IRI (see upper right part of Figure 10). But even here there is clearly no sign of even weak attraction between the *t*-Bu group and DMAP (no orange/red regions corresponding to negative $sign(\lambda_2)\rho$ values). Thus, we can conclude that only for the *i*-Pr_3Si group dispersive attraction is possible.

Until now, there was only one method for the selective 3–lithiation of DMAP, based on the utilization of sterically hindered Caubère's salt–the mixture of trimethylsilylmethyllithium with LiDMAE (Scheme 1).[21] Here we demonstrate that an even better result can be achieved by the simple usage of the excess of *t*-BuLi. This discovery allows the assumption that the previously reported lithiation of DMAP with Caubère's salt occurs in a similar fashion: the formation of a $Me_3SiCH_2(THF)_2Li$-LiDMAE-DMAP complex creates steric hindrance around the C2(6)–H bonds (Scheme 4b), allowing the excess of Me_3SiCH_2Li to perform selective C3(5)–H bond lithiation (see SI for details).

The simplicity of our approach opens convenient way to the selective C3-functionalization of DMAP. Thus, various electrophiles can be effectively used for this purpose (Table 5).

Table 5. C3(5)–functionalization of DMAP via lithiation with *t*–BuLi

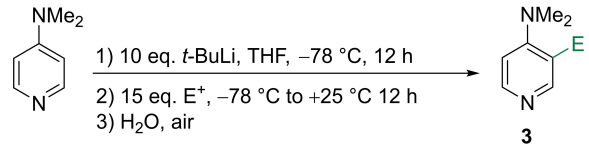

3

Run	E^+	Product	E	Isolated yield (%)
1	DMF	**3a**	CHO	91
2	MeOD	**3c**	D	95
3	Me_2S_2	**3d**	SMe	80

Conclusions

In summary, using quantum chemical calculations, we have demonstrated that the NMe_2 group of DMAP and its 1-substituted derivatives are unable to provide a directed *ortho*-metalation effect due to the strong conjugation with the pyridine ring. As a result, the interaction of these substrates with organometallic reagents is only controlled by steric availability and polarity of corresponding CH–bond. This opens possibility to flip the metalation of DMAP via the introduction of bulky substituents in position 1, which sterically blocks access to a more polar C2–H bond and thus allows for selective C3-functionalization. Using an intertwined approach of quantum chemical calculations and synthetic experiments, we have demonstrated that the size of the Me_3Si substituent is sufficient for this purpose, thus the lithiation of Me_3Si-DMAP with LDA and LTMP gives excellent C3-selectivity, with low yields, however. Much higher yields can be achieved with the utilization of *t*-BuLi as a stronger organometallic base. It was found that the coordination of *t*-BuLi to the pyridine nitrogen of DMAP provides a similar steric hindrance of the C2–H bond, allowing an even more selective C3–H lithiation without the use of any additional reagents. This simple approach allows convenient way to the selective C3-functionalization of DMAP. For the first time, we have demonstrated that the *i*-Pr_3Si moiety can serve as a directing group by relying on the dispersion interaction with an organometallic reagent. Despite the larger size in comparison to the Me_3Si group, this substituent provides a high yielding, excellent C2–H lithiation selectivity of *i*-Pr_3Si-

DMAP with LDA, LTMP and *t*-BuLi. This important finding opens the new perspective of the utilization of dispersion interactions for the selective lithiation of aromatic substrates.

Experimental Section

Computational Details

Computational resources were provided by the Computer Center of Saint-Petersburg University Research Park (http://www.cc.spbu.ru/). The calculations were carried out using the Gaussian16 software package.[41] Geometry optimizations and harmonic vibrational frequencies calculations were performed at the B3LYP/6-311++G(d,p) level of theory.[42,43] The Grimme dispersion correction D3 was included.[44] The total electron energy was refined at the B3LYP–D3(BJ)/6-311++G(d,p) level of theory. All structures were checked on the absence of imaginary harmonic vibrational frequencies. Solvent effects were accounted implicitly using the conductor-like polarizable continuum model (CPCM).

The MultiWFN[45] program was used for calculating the surfaces of electron density, electron localization function[26] and molecular electrostatic potential.[46] NBO analysis was performed using NBO 7.0 program. The visualization was performed using GaussView. The calculation of the accessible surface area and the volumes of the regions of dispersion attraction was performed using Matlab R2021b.

General

Tetrahydrofuran (THF) was dried over sodium/benzophenone. Liquid-state NMR experiments were performed using a Bruker Avance iii NMR spectrometer (400 MHz for ^{1}H and 100 MHz for ^{13}C) at the Center for Magnetic Resonance, St. Petersburg State University Research Park. Chemical shifts are referenced to TMS for ^{1}H and ^{13}C.

Single crystals of **3a** and **3c** were grown by slow evaporation of ethyl acetate solution at +25 °C. The single crystal X-ray diffraction data were collected using the SuperNova diffractometer equipped with a HyPix-3000 detector and a micro-focus Cu Ka radiation source (λ = 1.54184 Å) at temperature T = 100 (2) K at the Centre for X-ray Diffraction Studies, St. Petersburg State University Research Park. Using Olex216, the structure was solved with the SHELXT[47] structure solution pro-gram using Intrinsic Phasing and refined with the SHELXL[48] refinement package using Least Squares minimization.

Deposition Number(s) 2381185 (for **3a**), 2381187 (for **3c**), contain(s) the supplementary crystallographic data for this paper. These data are provided free of charge by the joint Cambridge Crystallographic Data Centre and Fachinformationszentrum Karlsruhe Access Structures service.

Synthesis

Preparation of F_3B-DMAP. 4-Dimethylaminopyridine (DMAP) (100 mg, 0.819 mmol) was dissolved in dry tetrahydrofuran (20 mL) in a flame dried round-bottomed flask. The flask was flushed with dry argon and sealed with a silicone septum. $F_3B{\cdot}Et_2O$ (104 μL, 0.819 mmol) was added dropwise at 0 °C using Hamilton syringe. The reaction mixture was stirred for 30 min to give clear solution of F_3B-DMAP with quantitative yield.

Preparation of Me_3Si-DMAP. DMAP (100 mg, 0.819 mmol) was dissolved in dry tetrahydrofuran (20 mL) in a flame dried round-bottomed flask. The flask was flushed with dry argon and sealed with a silicone septum. Me_3SiOTf (162 μL, 0.819 mmol) was added dropwise at 0 °C using Hamilton syringe. The reaction mixture was stirred for 30 min to give clear solution of $[Me_3Si\text{-}DMAP]^+OTf^-$ with quantitative yield.

Preparation of *i*–Pr_3Si-DMAP. DMAP (100 mg, 0.819 mmol) was dissolved in dry tetrahydrofuran (20 mL) in a flame dried round-bottomed flask. The flask was flushed with dry argon and sealed with a silicone septum. *i*–Pr_3SiOTf (228 μL, 0.819 mmol) was added dropwise at 0 °C using Hamilton syringe. The reaction mixture was stirred for 30 min to give clear solution of $[i\text{–}Pr_3Si\text{-}DMAP]^+OTf^-$ with quantitative yield.

General approach to the study of the lithiation of DMAP and its 1-substituted derivatives. The solution of organometallic reagent (LDA in THF, LTMP in THF or *t*-BuLi in pentane) was added dropwise to a solution of DMAP or its 1-substituted derivative (F_3B-DMAP, Me_3Si-DMAP or *i*-Pr_3Si-DMAP) using Hamilton syringe. The reaction mixture was stirred for required time, and the metalation was stopped by adding excess of dry DMF. Obtained mixture was stirred for 12 h at room temperature. The solvent was evaporated, and water (150 mL) was added. The products were extracted with dichloromethane (2×25 mL). The solvent was evaporated to dryness and the residue was subjected to NMR investigation without any purification. Formed 2-formyl-DMAP, 2,6-diformyl-DMAP, 3-formyl-DMAP, 3-Me_3Si-DMAP, were detected by the comparison of obtained NMR spectra with the published data.[21,49–51] Previously unknown 2-*i*-Pr_3Si-DMAP was prepared as described below.

2- (triisopropylsilyl)-4-dimethylaminopyridine (1b). The 1.7 M solution of *t*-BuLi in pentane (4.81 mL, 8.19 mmol) was added dropwise to the freshly prepared solution of *i*-Pr_3Si-DMAP in THF at −78 °C via syringe. The mixture was then stirred for 12 h at the same temperature. The reaction mixture was allowed to warm to room temperature over the next 6 h. Water (100 mL) was added. The product was extracted with dichloromethane (2×25 mL), the organic layer was dried over anhydrous Na_2SO_4 and evaporated under vacuum to dryness to give pure **1b** as pale-yellow crystals (yield 91 %).

^{1}H NMR (400 MHz, $CDCl_3$, 298 K): δ 1.14 (d, ^{3}J = 7.4 Hz, 18H), δ 1.56 (sep, ^{3}J = 7.4 Hz, 3H), δ 3.21 (s, 6H), δ 6.73 (dd, ^{3}J = 6.9 Hz, ^{4}J = 2.9 Hz, 1H), δ 6.76 (d, ^{4}J = 2.9 Hz, 1H), δ 8.49 (d, ^{3}J = 6.9 Hz, 1H) ppm.

$^{13}C\{^{1}H\}$ NMR (100 MHz, $CDCl_3$, 298 K): δ 11.0, 18.6, 38.9, 105.5, 114.4, 149.7, 152.3, 163.0 ppm.

^{29}Si NMR (79 MHz, $CDCl_3$, 298 K): δ 4.7 (s, Si(*i*-Pr)$_3$) ppm.

HR-ESI MS: m/z, 279.2252. Calculated for $C_{16}H_{31}N_2Si$ $[M+H]^+$ = 279.2251.

General procedure for C-3 functionalization of DMAP. DMAP (100 mg, 0.82 mmol) in THF (20 mL) was placed in a flame dried round-bottomed flask. The flask was flushed with dry argon and sealed with a silicone septum. The 1.7 M solution of *t*-BuLi in pentane (4.81 mL, 8.19 mmol) was added dropwise at −78 °C via syringe. The mixture was then stirred for 12 h at the same temperature. 15 equiv. of the appropriate electrophile (DMF for **3a**, Me_2S_2 for **3b** and MeOD for **3c**) were added. The reaction mixture was allowed to warm to room temperature over the next 12 h. Water (100 mL) was added. The product was extracted with dichloromethane (2×25 mL), the organic layer was dried over anhydrous Na_2SO_4 and evaporated under vacuum to dryness. The residue was purified by TLC on Al_2O_3 and AcOEt as eluent.

3-formyl-4-dimethylaminopyridine (3 a). $R_f = 0.7$, yellow solid (yield 91 %). Spectral data is in agreement with previously published.[52]

^{1}H NMR (400 MHz, $CDCl_3$, 298 K): δ 3.01 (s, 6H), 6.66 (d, $^3J = 6.1$ Hz, 1H), 8.24 (d, $^3J = 6.1$ Hz, 1H), 8.60 (s, 1H), 9.91 (s, 1H) ppm.

3-*d*-4-dimethylaminopyridine (3c). ($R_f = 0.9$), colorless solid (yield 95 %). Spectral data is in agreement with previously published.[53]

^{1}H NMR (400 MHz, $CDCl_3$, 298 K): δ 2.90 (s, 6H), 6.40 (d, $^3J = 6.0$ Hz, 1H), 8.31 (d, $^3J = 6.0$ Hz, 1H), 8.31 (s, 1H) ppm.

^{13}C NMR (100 MHz, $CDCl_3$, 298 K): δ 38.9, 106.5, 149.5, 149.6, 154.1 ppm.

3-methylthio-4-dimethylaminopyridine (3 d). $R_f = 0.9$, yellow solid (yield 80 %). Spectral data is in agreement with previously published.[21]

^{1}H NMR (400 MHz, $CDCl_3$, 298 K): δ 2.46 (s, 6H), δ 2.98 (s, 6H), 6.75 (d, $^3J = 5.5$ Hz, 1H), 8.23 (d, $^3J = 5.5$ Hz, 1H), 8.32 (s, 1H) ppm.

2-*tert*-butyl-4-dimethylaminopyridine (4). DMAP (81 mg, 0.663 mmol) was dissolved in dry tetrahydrofuran (16.2 mL) in a flame dried round-bottomed flask. The flask was flushed with dry argon and sealed with a silicone septum. 1.7 M solution of *t*-BuLi in pentane (0.59 mL, 0.994 mmol) was added dropwise at −24 °C via syringe. The reaction mixture was stirred for 24 h. The solvent was evaporated, and water (60 mL) was added. The product was extracted with dichloromethane (3×15 mL), the organic layer was dried over anhydrous Na_2SO_4 and evaporated under vacuum to dryness. The residue was purified by column chromatography on Al_2O_3 and mixture of AcOEt–petroleum ether (2 : 1, v/v) as the eluent to yield 9.2 mg (7.8 %) of **4** as colorless oil.

^{1}H NMR (400 MHz, $CDCl_3$, 298 K): δ 1.38 (s, 9H), 3.02 (s, 6H), 6.37 (dd, $^2J = 5.9$, $^3J = 2.6$ Hz, 1H), 6.56 (d, $^2J = 2.5$, 1H), 8.25 (d, $^2J = 5.9$ Hz, 1H) ppm.

^{13}C NMR (100 MHz, $CDCl_3$, 298 K): δ 30.3, 37.2, 39.2, 101.7, 104.1, 148.7, 154.9, 169.3 ppm.

HR-ESI MS: m/z, 179.1543. Calculated for $C_{11}H_{19}N_2$ $[M+H]^+ =$ 179.1543.

Acknowledgements

This work was supported by the Russian Science Foundation (project 21–73-10040). The authors thank Mr. Daniel Raith for proofreading the paper with regard to the English language. Open Access funding enabled and organized by Projekt DEAL.

Conflict of Interests

The authors declare no conflict of interest.

Data Availability Statement

The data that support the findings of this study are available in the supplementary material of this article.

Keywords: Dispersion interaction · Metalation · Steric hindrance · Pyridine · Organolithium

[1] Y. Hamada, *in Pyridine*, InTech, **2018**.
[2] S. De, A. Kumar S K, S. K. Shah, S. Kazi, N. Sarkar, S. Banerjee, S. Dey, *RSC Adv.* **2022**, *12*, 15385–15406.
[3] X. F. Wu, *Transition Metal-Catalyzed Pyridine Synthesis: Transition Metal-Catalyzed Heterocycle Synthesis Series*, Elsevier **2016**.
[4] T. Nagata, Y. Obora, *Asian J. Org. Chem.* **2020**, *9*, 1532–1547.
[5] Y. Nakao, *Synthesis (Stuttg).* **2011**, *2011*, 3209–3219.
[6] *Polar Organometallic Reagents: Synthesis, Structure, Properties and Applications* (Eds: A. E. H. Wheatley, M. Uchiyama), John Wiley & Sons Ltd, Chichester **2022**.
[7] Z. Chai, W. X. Zhang, *Organometallics* **2022**, *41*, 3455–3477.
[8] G. Wu, M. Huang, *Chem. Rev.* **2006**, *106*, 2596–2616.
[9] F. Totter, P. Rittmeyer, *Organometallics Synth.* (Ed: M. Schlosser), John Wiley & Sons, Inc., Hoboken, NJ, USA **2013**, 167–194.
[10] M. Schlosser, *Met. Azines Diazines* (Eds: M. Schnürch, M. D. Mihovilovic), Springer Berlin Heidelberg **2013**, 171–222.
[11] G. Illuminati, F. Stegel, *Adv. Heterocycl. Chem.* **1983**, *34*, 305–444.
[12] S. V. Kessar, P. Singh, *Chem. Rev.* **1997**, *97*, 721–738.
[13] P. Gros, Y. Fort, P. Caubère, *J. Chem. Soc. Perkin. Trans.* **1997**, *1*, 3597–3600.
[14] J. Verbeek, L. Brandsma, *J. Org. Chem.* **1984**, *49*, 3857–3859.
[15] A. B. Bellan, P. Knochel, *Angew. Chemie - Int. Ed.* **2019**, *58*, 1838–1841.
[16] V. Snieckus, *Chem. Rev.* **1990**, *90*, 879–933.
[17] M. Schlosser in Organometallics Synth. *A Man.*, John Wiley & Sons, Inc., Hoboken, NJ, USA **2013**, 1–352.
[18] P. Gros, Y. Fort, *European J. Org. Chem.* **2002**, *2002*, 3375–3383.
[19] T. Saied, C. Demangeat, A. Panossian, F. R. Leroux, Y. Fort, C. Comoy, *European J. Org. Chem.* **2019**, *2019*, 5275–5284.
[20] D. Cuperly, P. Gros, Y. Fort, *J. Org. Chem.* **2002**, *67*, 238–241.
[21] P. C. Gros, A. Doudouh, C. Woltermann, *Chem. Commun.* **2006**, 2673–2674.
[22] A. S. Antonov, V. G. Bardakov, V. V. V. Mulloyarova, *J. Organomet. Chem.* **2020**, *906*, 121068.
[23] A. S. Antonov, A. F. Pozharskii, V. A. Ozeryanskii, A. Filarowski, K. Y. Suponitsky, P. M. Tolstoy, M. A. Vovk, *Dalt. Trans.* **2015**, *44*, 17756–17766.
[24] J. Bräckow, K. T. Wanner, *Tetrahedron* **2006**, *62*, 2395–2404.
[25] K. Akiba, Y. Iseki, M. Wada, *Tetrahedron Lett.* **1982**, *23*, 3935–3936.
[26] A. Savin, R. Nesper, S. Wengert, T. F. Fässler, *Angew. Chemie Int. Ed. English* **1997**, *36*, 1808–1832.
[27] T. Lu, Q. Chen, *Chemistry–Methods* **2021**, *1*, 231–239.
[28] T. Lu, Q. Chen in Compr. *Comput. Chem.*, Elsevier **2024**, 240–264.
[29] R. F. W. Bader, *Chem. Rev.* **1991**, *91*, 893–928.
[30] B. Lee, F. M. Richards, *J. Mol. Biol.* **1971**, *55*, 379–400.
[31] A. Shrake, J. A. Rupley, *J. Mol. Biol.* **1973**, *79*, 351–371.
[32] E. R. Chakalov, E. Y. Tupikina, D. M. Ivanov, E. V. Bartashevich, P. M. Tolstoy, *Molecules* **2022**, *27*, 4848.
[33] H. J. Reich, *Chem. Rev.* **2013**, *113*, 7130–7178.
[34] L. Rummel, P. R. Schreiner, *Angew. Chemie Int. Ed.* **2024**, *63*, e202316364.
[35] S. Rösel, H. Quanz, C. Logemann, J. Becker, E. Mossou, L. Cañadillas-Delgado, E. Caldeweyher, S. Grimme, P. R. Schreiner, *J. Am. Chem. Soc.* **2017**, *139*, 7428–7431.
[36] S. Rösel, J. Becker, W. D. Allen, P. R. Schreiner, *J. Am. Chem. Soc.* **2018**, *140*, 14421–14432.
[37] J. Gramüller, R. M. Gschwind, *Acc. Chem. Res.* **2023**, *56*, 2968–2979.
[38] J. Gramüller, M. Franta, R. M. Gschwind, *J. Am. Chem. Soc.* **2022**, *144*, 19861–19871.
[39] H. F. König, L. Rummel, H. Hausmann, J. Becker, J. M. Schümann, P. R. Schreiner, *J. Org. Chem.* **2022**, *87*, 4670–4679.
[40] T. Lu, Q. Chen, *J. Mol. Model.* **2020**, *26*, 315.
[41] Gaussian 16, Revision C.01, M. J. Frisch, G. W. Trucks, H. B. Schlegel, G. E. Scuseria, M. A. Robb, J. R. Cheeseman, G. Scalmani, V. Barone, G. A. Petersson, H. Nakatsuji, X. Li, M. Caricato, A. V. Marenich, J. Bloino, B. G. Janesko, R. Gomperts, B. Mennucci, H. P. Hratchian, J. V. Ortiz, A. F. Izmaylov, J. L. Sonnenberg, D. Williams-Young, F. Ding, F. Lipparini, F. Egidi, J. Goings, B. Peng, A. Petrone, T. Henderson, D. Ranasinghe, V. G. Zakrzewski, J. Gao, N. Rega, G. Zheng, W. Liang, M. Hada, M. Ehara, K. Toyota, R. Fukuda, J. Hasegawa, M. Ishida, T. Nakajima, Y. Honda, O. Kitao, H. Nakai, T. Vreven, K. Throssell, J. A. Montgomery, Jr., J. E. Peralta, F. Ogliaro, M. J. Bearpark, J. J. Heyd, E. N. Brothers, K. N. Kudin, V. N. Staroverov, T. A. Keith, R. Kobayashi, J. Normand, K. Raghavachari, A. P. Rendell, J. C. Burant, S. S. Iyengar, J. Tomasi, M. Cossi, J. M. Millam, M. Klene, C. Adamo, R. Cammi, J. W. Ochterski, R. L. Martin, K. Morokuma, O. Farkas, J. B. Foresman, D. J. Fox, Gaussian, Inc., Wallingford CT, 2016.
[42] A. D. Becke, *J. Chem. Phys.* **1992**, *96*, 2155–2160.

[43] C. Lee, W. Yang, R. G. Parr, *Phys. Rev. B* **1988**, *37*, 785–789.
[44] S. Grimme, S. Ehrlich, L. Goerigk, *J. Comput. Chem.* **2011**, *32*, 1456–1465.
[45] T. Lu, F. Chen, *J. Comput. Chem.* **2012**, *33*, 580–592.
[46] J. Zhang, *J. Chem. Theory Comput.* **2018**, *14*, 572–587.
[47] G. M. Sheldrick, *Acta Crystallogr. Sect. A Found. Crystallogr.* **2015**, *71*, 3–8.
[48] G. M. Sheldrick, *Acta Crystallogr. Sect. A Found. Crystallogr.* **2008**, *64*, 112–122.
[49] R. López-Rodríguez, A. Ros, R. Fernández, J. M. Lassaletta, *J. Org. Chem.* **2012**, *77*, 9915–9920.
[50] T. F. S. Ali, K. Iwamaru, H. I. Ciftci, R. Koga, M. Matsumoto, Y. Oba, H. Kurosaki, M. Fujita, Y. Okamoto, K. Umezawa, M. Nakao, T. Hide, K. Makino, J. I. Kuratsu, M. Abdel-Aziz, G. E. D. A. A. Abuo-Rahma, E. A. M. Beshr, M. Otsuka, *Bioorganic Med. Chem.* **2015**, *23*, 5476–5482.
[51] T. Poisson, S. Oudeyer, V. Levacher, *Tetrahedron Lett.* **2012**, *53*, 3284–3287.
[52] R. López-Rodríguez, A. Ros, R. Fernández, J. M. Lassaletta, *J. Org. Chem.* **2012**, *77*, 9915–9920.
[53] T. Poisson, M. Penhoat, C. Papamicaël, G. Dupas, V. Dalla, F. Marsais, V. Levacher, *Synlett.* **2005**, 2285–2288

Manuscript received: September 12, 2024
Accepted manuscript online: November 12, 2024
Version of record online: ■■, ■■

RESEARCH ARTICLE

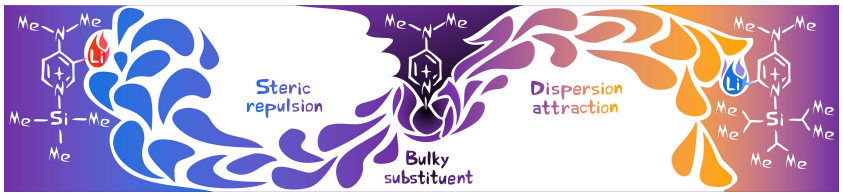

*V. A. Verkhov, A. N. Gubanova, D. I. Tonkoglazova, E. Y. Tupikina, A. S. Antonov**

We demonstrate the effective utilization of steric interactions for flipping the lithiation of 4-dimethylaminopyridine (DMAP). Introduction of a Me_3Si substituent to the position 1 of DMAP or simple complexation with t-BuLi allows selective C3-lithiation, due to the steric hindrance of a C2–H bond. The utilization of i-Pr_3Si substituent leads to exclusive C2-functionalization due to the dispersion interactions with organometallic bases.